



# Numerical simulation of 3-D mantle flow evolution in subduction zone environments in relation to seismic anisotropy beneath the eastern Mediterranean region

Judith M. Confal<sup>a,\*</sup>, Manuele Faccenda<sup>b</sup>, Tuna Eken<sup>a</sup>, Tuncay Taymaz<sup>a</sup>

<sup>a</sup> Department of Geophysical Engineering, The Faculty of Mines, Istanbul Technical University, 34469 Maslak, Sariyer, Istanbul, Turkey

<sup>b</sup> Department of Geoscience, University of Padua, Italy

## ARTICLE INFO

### Article history:

Received 17 November 2017  
Received in revised form 23 May 2018  
Accepted 4 June 2018  
Available online xxxx  
Editor: P. Shearer

### Keywords:

Aegean  
Eastern Mediterranean  
kinematics of upper mantle deformation  
seismic anisotropy  
shear wave splitting  
subduction zone processes

## ABSTRACT

Seismic anisotropy is a key parameter in understanding subduction zone dynamics in relation to the recent deformation history. It is usually controlled by the mantle flow patterns resulting from the dynamic interactions between a relatively dense subducting oceanic plate and the surrounding mantle. A proper modelling of mantle flow in subduction systems helps our understanding of the seismic anisotropy source, strength and evolution in time. This study further examines shear wave splitting parameters, one of the most well established measuring methods of seismic anisotropy, and their anisotropy source, based on 3-D geodynamic modelling, applied to the eastern Mediterranean Sea and Anatolia. Our model setting is chosen to be a first order representation of the present-day tectonic setting as it consists of a deforming Anatolian micro-plate, that is indented by slow moving African and Arabian plates, and an oceanic plate in between. The retreat of the slab in the Aegean region, the alleged tear in the subducting slab close to the Cyprus trench and the break-off in the slab in eastern Anatolia are considered in our modelling study in order to further explore their influence on mantle flow and splitting parameters. The synthetically calculated fast polarization directions (FPDs) mostly showed a reasonable matching with those inferred from previous seismological observations that are mainly SKS splitting measurements. Regions of FPD similarities between synthetic and observed shear waves mostly indicate N–S to NE–SW orientations of fast shear waves, which are parallel to the extension in the back-arc region and in general perpendicular to the trench. The pattern of FPDs seems to be more complex nearby the trench. Our modelling results suggest that the development of a tear in the African slab and the detachment occurring within the Arabian plate (break-off) appear to have a significant influence on the FPDs due to stronger mantle flow through the slab windows. The mantle flow through the tear close to Cyprus and the break-off in the East can be identified clearly, despite their recent appearances. A circular pattern around the edges of the slab can be observed as well as disruptions of the overall general fast polarization direction due to the flow through the tear.

© 2018 Elsevier B.V. All rights reserved.

## 1. Introduction

A proper modelling of 3-D mantle flow evolution beneath the eastern Mediterranean, the Aegean and Anatolia, will significantly contribute to our understanding of the complex dynamics of this region, involving subduction zones, back-arc spreading, collisional and extrusion tectonics (Fig. 1). Indeed, by having a proper knowledge of upper mantle flow history, recent kinematics and dynamic patterns of the mantle can be reconstructed (e.g. Faccenna et al., 2013; Sternai et al., 2014). Comparing synthetic data with ob-

servational constraints, i.e., from seismic anisotropy, tomographic models and geodetic measurements, can comprehensively help us to illuminate the evolution of mantle flow patterns as well as their influence on subduction zone environments (e.g. Park and Levin, 2002). Seismic anisotropy, generated by strain-induced lattice preferred orientations (LPOs) of olivine, the most abundant mineral in the upper mantle, is widely used to infer upper mantle flow characteristics. Observations on the splitting of shear waves into fast and slow components are the most common and direct approach to recover a path-integrated fast wave orientation and the strength of anisotropy. The fast wave is orthogonal to the slow one and is polarized in the plane with the highest shear wave velocity (fast polarisation direction, FPD). The time delay (TD) between the

\* Corresponding author.

E-mail address: judithconfal@gmail.com (J.M. Confal).

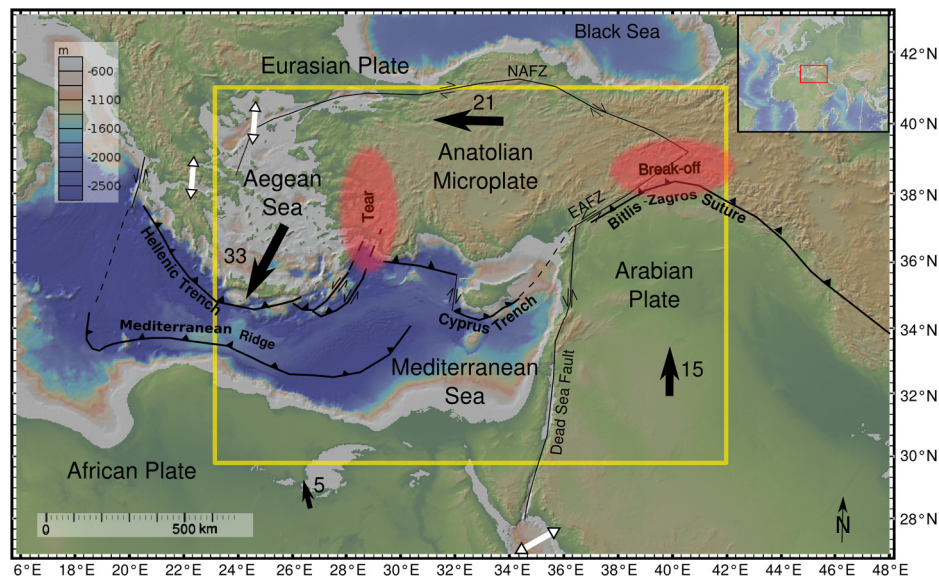


**Fig. 1.** Active tectonic map of the eastern Mediterranean (Global Multi-Resolution Topography map from GeoMapApp, <http://www.geomapp.org>) and sketch of main active tectonic features after Dilek and Altunkaynak (2009, and references therein) with principal movements of the plates in respect to a stable Eurasian plate after Le Pichon and Kreemer (2010). Black solid arrows show directions of plate movements with their respective plate velocities in mm/yr and white arrows represent extensional regimes (about 15 mm/yr in the North Aegean and the Gulf of Corinth and 17 mm/yr in the Red Sea). The yellow square represents the modelled region. The transparent red areas show the supposed locations of the slab tear in western Turkey and the slab break-off in eastern Turkey. Lines with triangles show thrust faults and subduction zones, normal lines with paired arrows are strike slip boundaries. NAFZ and EAFZ represent the North and East Anatolian Fault Zones, respectively. (For interpretation of the colours in the figure(s), the reader is referred to the web version of this article.)

fast and slow wave is proportional to the thickness and the intrinsic anisotropy of the medium where the shear wave is propagating through. Early studies (Long and Silver, 2009) tend to link flow patterns with the distribution of anisotropy that were inferred mainly from SKS, SKKS and local/teleseismic S waves. A global compilation of splitting observations has indicated that the FPDs in subduction systems are mostly trench-perpendicular in the back-arc region and trench-parallel closer to the trench (Long and Silver, 2009).

Apart from mantle flow patterns, Karato et al. (2008) claimed that other parameters such as temperature, water content and deviatoric stress influence the LPO of olivine. Apparent anisotropy, related to isotropic compositional heterogeneities, could constitute an additional anisotropy source (e.g. Babuska and Cara, 1991). Traditionally, modelling studies assume time-independent, steady-state flow dynamics to calculate mantle fabrics and the associated anisotropy (e.g. Becker, 2006). This method has been shown to be effective in global intra-oceanic settings (e.g. Pacific and Atlantic ocean) where plate motions and shallow mantle flow has been stable over the past 43 Myrs (Faccenna et al., 2013, e.g.). Recently, Faccenna and Capitanio (2013, and references therein) have extended this methodology to account for the non-steady state deformation, likely to be expected at subduction zones, characterized by trench and slab lateral migration.

Faccenna and Capitanio (2013) identified two types of anisotropic domains in the modelled sub-slab mantle: trench-parallel in the deeper upper mantle related to the diverging toroidal mantle flow component, and trench-perpendicular within the overlying and dip-parallel mantle that is entrained at depth by the subducting plate. Another significant result from their model is, that the strength of sub-slab trench-parallel splitting directions are prone to be manifested by the amount of the retreat motion rather than the migration rate of the slab. Faccenna and Capitanio (2013), modelled the upper mantle anisotropy for 3-D subduction models with different geometries. Synthetically computed splitting parameters agree overall with observations from different subduction zones if the mantle flow (and thus the olivine fast axis) is sub-horizontal, while the fit degrades in proximity to the trench, where the flow is dipping parallel to the slab. In particular, their

study was successful in modelling the circular FPD pattern at the edges of a subducting slab and the trench-perpendicular FPDs in the back-arc regions. The trench-parallel FPDs commonly observed at fore-arcs were reproduced only in models that develop a strong sub-slab trench-parallel fabric in response to a sustained slab rollback and pure shear deformation (Faccenna and Capitanio, 2013).

Our aim in this study is to apply a similar modelling approach to the complicated eastern Mediterranean subduction system, where the present-day geological setting (Fig. 1) shows an African plate subducting underneath a stable Eurasia and a fast moving Anatolian microplate (Reilinger et al., 2006). In the initial model set up, we consider crustal thicknesses, widths of plates, Moho depths and the expected time frame of the subduction process, based on available literature for a realistic approach, to model the geodynamics of the region. However, it is also important to note that this study offers only a first order approximation of the presumed mantle flow and strain pattern in the mantle in relation to the shear-wave splitting parameters, rather than exploring the exact geodynamic evolution of the subduction process and its corresponding tectonic setting in the eastern Mediterranean region.

### 1.1. Tectonic setting of the region

The eastern Mediterranean region is one of the most tectonically active regions in the world. Following the conversion of Africa and Eurasia, the Ionian oceanic lithosphere continues to subduct beneath Eurasia while the Anatolian plateau escapes westwards. The region is characterized by two different active subduction systems (Cyprus and Hellenic), a collision zone around the Bitlis–Zagros suture, an extensional region in the Aegean Sea, and an extruding Anatolian microplate (e.g. Le Pichon and Kreemer, 2010).

Tectonic history reconstructions of Van Hinsbergen et al. (2005) dated the closing of the Pindos (Neo-Tethys) ocean at around 34 Myrs. Seismic tomography, geological models and 3-D numerical models (e.g. Wortel and Spakman, 2000; Jolivet and Faccenna, 2000; Menant et al., 2016) suggest that the extension in the northern Aegean started in the Oligocene–Miocene around 25 to 35 Myrs ago and the recent phase of extension is about

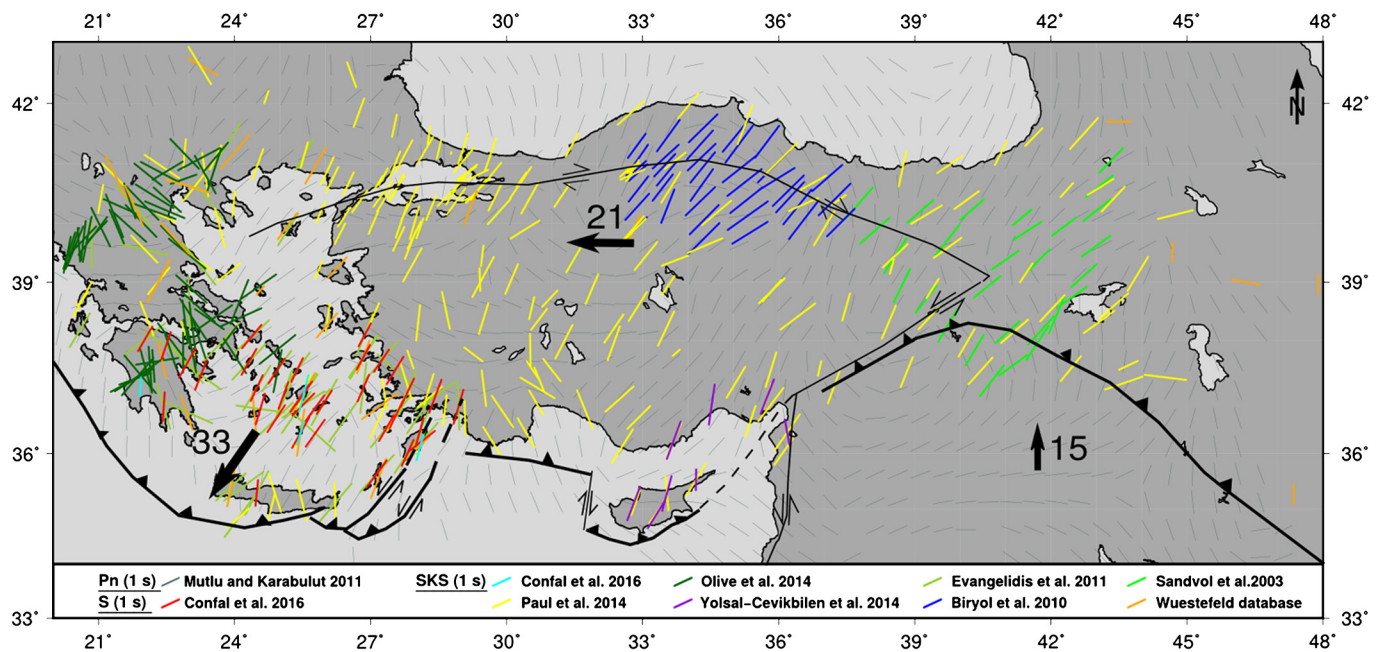


**Fig. 2.** Anisotropy parameters from previous Pn-tomography (Mutlu and Karabulut, 2011), direct S-wave (Confal et al., 2016) and SKS-wave studies in the eastern Mediterranean from the splitting data base of Wüstefeld and Bokelmann (2007) and (Sandvol et al., 2003; Biryol et al., 2010; Evangelidis et al., 2011; Yolsal-Çevikbilen, 2014; Paul et al., 2014; Olive et al., 2014; Confal et al., 2016). Black solid arrows show directions of plate movements with their respective plate velocities in mm/yr.

10–15 Myrs old (Wortel and Spakman, 2000). Govers and Fichtner (2016) proposed a fragmentation of the slab in the Eocene–Miocene, leading to the roll-back in the Aegean (Hellenic slab) and the steepening of the Cyprus slab based on 3-D high-resolution S-wave speed distribution in the region. Jolivet et al. (2015) dated the beginning of slab tearing close to the Cyprus trench at around 15 Myrs, due to fast extension. Low velocity anomalies, resolved in southwestern Turkey, based on body and surface wave tomography studies (Taymaz, 1996; Biryol et al., 2011; Govers and Fichtner, 2016), tend to support the idea of a North-South vertical tear within the African slab, which propagates laterally. Low velocity anomalies, from 50–100 km down to a depth of about 800 km evidenced the indication of this tear in the slab between the Cyprus and the Hellenic trench. Moreover, there might be even evidence for a smaller tear in the Cyprus trench (Biryol et al., 2011). A steepening of the African slab from the west to the east in the Aegean Sea is evident from tomography images (e.g. Wortel and Spakman, 2000).

On the basis of the reconstruction of geodynamic evolution, Jolivet and Faccenna (2000) claimed that Anatolia and Arabia collided around 30 to 35 Myrs ago. In the East, where the Anatolian and the Arabian plate collide, the common consensus at the moment is that a break-off of the Arabian slab is mainly responsible for the formation of the east Anatolian plateau (domal uplift) and volcanism (e.g. Keskin, 2003). He describes the Anatolian crust being still actively deforming, while the northward subducting oceanic lithosphere of the Arabian plate steepened, the mantle lithosphere delaminated (Göğüş and Pysklywec, 2008) and parts of the slab detached itself from the accretionary wedge. Keskin (2003) dates the initiation of the break-off around 11–13 Myrs ago. A recent high resolution S-receiver function study performed by Kind et al. (2015) indicated that the seismological lithosphere–asthenosphere boundary (LAB) could not be deeper than 100–120 km in eastern Turkey. Faccenna et al. (2006) interpreted the sharp transition between fast and slow Pn-velocities around the Central Anatolian Fault Zone as the edge of a second slab window, continuing to the west. For modelling purposes we will consider the widely accepted theory of just one slab window in the East below the collision zone.

Pasyanos and Walter (2002) obtained crustal thicknesses for the African plate around 40 km and for the Arabian plate 25–35 km. The Anatolian plate is about 30 km thick in the West (e.g. Vanacore et al., 2013, and references therein), 37–47 km in central Anatolia and 38–55 km thick on the eastern Anatolian Plateau, as it simply indicates a west-to-east crustal thickening (e.g. Mutlu and Karabulut, 2011; Vanacore et al., 2013). Due to the retreat the crust of the Aegean Sea is thinner (about 25 km, Tirel et al., 2004) than surrounding plates.

Geodetic observations showed a northward movement of Africa, by about 5 mm/yr with respect to Eurasia and 15 mm/yr for the Arabian plate (Reilinger et al., 2006; Le Pichon and Kreemer, 2010). The Anatolian plate rotates counterclockwise at around 18–25 mm/yr and the Aegean domain migrates at about 33 mm/yr to the southwest. A proper understanding of the relative contribution to the present-day active deformation from both the continental collision of the Arabian and Eurasian plate triggering a westward material extrusion in Anatolia (e.g. Le Pichon and Kreemer, 2010) and the pull in the West due to the fast extension in the Aegean domain still remains debated (e.g. Sternai et al., 2014). At present it is evident from geodetic observations that the retreat of the southwestward dipping Hellenic slab produces an extensional regime of about 15 mm/yr in the Aegean Sea. Faccenna et al. (2003) favoured the orogenic collapse model, triggered by slab roll-back as the origin of the fast extension. Jolivet et al. (2013, and references therein) enhanced this theory by adding slab tearing, which became more plausible in recent years owing to the advances in GPS technology. In this study we consider the roll-back mechanism as an influential parameter on the mantle flow dynamics.

### 1.2. Anisotropic pattern of the region

Early SKS- and S-wave splitting studies performed in the eastern Mediterranean and Anatolia (Sandvol et al., 2003; Biryol et al., 2010; Evangelidis et al., 2011; Paul et al., 2014; Olive et al., 2014; Yolsal-Çevikbilen, 2014; Confal et al., 2016) have clearly indicated almost consistent NE–SW oriented anisotropic directions in the upper mantle and crust with sub-lithospheric origin (Fig. 2). In the

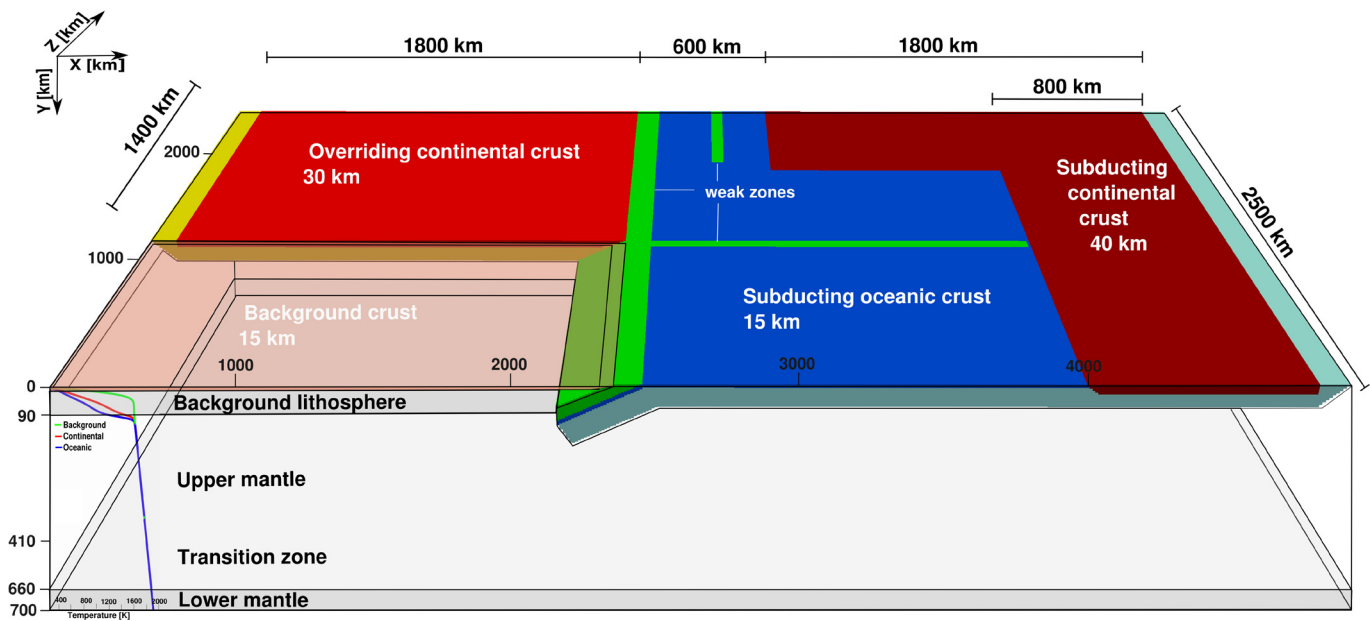


**Fig. 3.** Initial model set-up and compositions of the plates. Widths and thicknesses of the plates are indicated in km. Weak zones are shown in light green. Yellow and light blue layers resemble the lithospheric mantle of the overriding and subducting plates, respectively. The geotherms for the 150 Myrs old oceanic plate (blue), 70 Myrs old overriding continental plate and 5 Myrs old background (green) are shown in the lower left corner of the model.

western part of the study area and back-arc region FPDs are mostly NNE–SSW oriented with high TDs, while FPDs become rather NE–SW directed to the east and far from the trench with lower TDs. In southwestern Turkey, where the tear in the slab is suspected, the lateral variations of splitting parameters become more complicated (Paul et al., 2014). The dominant characteristics of the FPD distribution in the Aegean Sea is a trench-perpendicular pattern. Furthermore, Evangelidis et al. (2011) found a trench-parallel FPD pattern in the fore-arc region of the Aegean, but this is not supported by recent studies (Paul et al., 2014; Confal et al., 2016). On the Peloponnes and the Greek mainland Olive et al. (2014) and Evangelidis (2017) observed very complex trench-normal/parallel FPDs structures. They argue that these patterns are mainly affected by local changes beneath and above the slab due to return flow. Trench-parallel FPDs in the fore-arc region at shallow depth (<50 km) and trench-normal FPDs in sub-slab depths at the trench, might indicate a tear in the lower slab (Evangelidis, 2017).

Based on anisotropic inversion of surface waves, Endrun et al. (2011) revealed N–S directed, strain-related anisotropy parallel to the extension in the lithosphere of the northern Aegean and NE–SW directed anisotropy in the central Aegean crust from Miocene paleo-extension. A tomography study by Çubuk-Sabuncu et al. (2017) reported strong radial anisotropy throughout the crust of western Turkey and Mutlu and Karabulut (2011) observed that fast directions of Pn waves in the crust are consistent with SKS- and S-wave studies, especially in the central Aegean Sea, eastern Anatolia and central Turkey. Small differences, especially close to the trench, in the northern part of the Anatolian plate and western Turkey are prominent since active tectonics strongly affect Pn-waves in the crust.

## 2. Numeric modelling

Following the first 2-D steady-state models, dynamic recrystallisation and plastic deformation were included to study strain-induced anisotropy in the upper mantle (e.g. Becker, 2006), but the mantle flow is still seen as steady-state. These methods are problematic when it comes to subduction zones, which develop and change the flow pattern over their evolution. In this study, we ap-

ply the numerical modelling method, first introduced and modified for inter-compatibility of various modelling steps, computational speed, 3-D Cartesian geometry and time varying strain-induced anisotropy by Faccenda and Capitanio (2013). To calculate shear wave splitting parameters, it considers the full development of the mantle flow and anisotropy in the upper mantle that has resulted from the recent evolution of slab roll-back and tearing (about 30 Myrs) within the eastern Mediterranean subduction zone system. Prior to calculating SKS splitting parameters, two modelling steps are performed.

### 2.1. Mantle flow modelling

3-D petrological-thermo-mechanical models of subduction have been carried out with I3MG, which is based on a mixed Eulerian–Lagrangian Finite Difference scheme (Gerya, 2009; Faccenda, 2014). We set up a model resembling to a first order the subduction of a branch of the Neo-Tethys ocean (subducting oceanic plate), which still subducts in the eastern Mediterranean region along the Hellenic trench underneath Eurasia (overriding continental plate) and continues east towards the collisional area of the Anatolian and Arabian continental plates.

Our model has dimensions of  $(x, y, z) = 5000 \times 700 \times 2500$  km ( $245 \times 69 \times 149$  nodes and about  $20.4 \times 10.2 \times 16.8$  km spatial resolution), with  $y$  being the vertical direction. In the initial model (Fig. 3) the lithosphere reaches 90 km depth, as being consistent with the 80–100 km lithospheric thickness modelled beneath Anatolia by Kind et al. (2015) and is a common assumption in geodynamic modelling studies in the region (e.g. Sternai et al., 2014). Crustal thicknesses used for continental and oceanic crusts in our study are primarily based on Pasyanos and Walter (2002). Detailed layer thicknesses and information for each layer can be found in Table 1. The subducting continental plate (representing Arabia) has a crustal thickness of 40 km, a width of 700 km and is 1000 km longer than the plate occupying the remaining part (representing Africa), which has a width of 1800 km. The subducting oceanic crust is 15 km thick, due to resolution restrictions. Brittle weakening is imposed to ensure lubrication at plate boundaries. The oceanic plate terminates with a 200 km long slab dipping at about

**Table 1**  
Rheological parameters of the different layers. AD, n, E and V are flow law parameters after (Ranalli, 1995). V is 1 J/bar for all materials. The viscosity of the lower mantle is set constant. UM is the upper mantle and TZ represents the transition zone.

Geological unit	Effective thickness [km]		Geotherm [Myrs]	Viscosity [Pa s]	Friction coeff. [-]	$A_D$ [Pa s]	$n$ [-]	E [J]
Lithosphere	<u>Crust</u>	<u>Mantle</u>						
Background	15		5	$10^{18a}$	0.020/0.005 <sup>c</sup>	$1.97 \cdot 10^{17}$	2.3	$1.54 \cdot 10^5$
Background		75	5	$10^{18}/10^{24b}$	0.600/0.400 <sup>c</sup>	$3.98 \cdot 10^{16}$	3.5	$5.32 \cdot 10^5$
Subducting oceanic + slab	15		150	$10^{18}/10^{24b}$	0.020/0.005 <sup>c</sup>	$1.97 \cdot 10^{17}$	2.3	$1.54 \cdot 10^5$
Subducting oceanic + slab		75	150	$10^{18}/10^{23b}$	0.600/0.400 <sup>c</sup>	$3.98 \cdot 10^{16}$	3.5	$5.32 \cdot 10^5$
Subducting continental	40		150	$10^{18}/10^{24b}$	0.150	$1.97 \cdot 10^{17}$	2.3	$1.54 \cdot 10^5$
Subducting continental		50	150	$10^{18}/10^{23b}$	0.600/0.400 <sup>c</sup>	$3.98 \cdot 10^{16}$	3.5	$5.32 \cdot 10^5$
Overriding continental	30		70	$10^{18}/10^{22b}$	0.010	$1.97 \cdot 10^{17}$	2.3	$1.54 \cdot 10^5$
Overriding continental		60	70	$10^{18}/10^{22b}$	0.200/0.100 <sup>c</sup>	$3.98 \cdot 10^{16}$	3.5	$5.32 \cdot 10^5$
Weak zones		90	150	$10^{18}$	0.600/0.400 <sup>c</sup>	–	–	–
UM + TZ		570	Adiabatic	$10^{18}/10^{24b}$	0.600/0.400 <sup>cb</sup>	$3.98 \cdot 10^{16}$	3.5	$5.32 \cdot 10^5$
Lower mantle		40	Adiabatic	$10^{23}$	0.600/0.400 <sup>c</sup>	–	–	–

<sup>a</sup> No upper cut-off due to small friction coeff.

<sup>b</sup> Upper/lower cut-off values.

<sup>c</sup> Low/high strain.

30° underneath a continental plate (representing Anatolia). A weak lithosphere (background lithosphere), that facilitates retreat and lateral extrusion of the upper plate (background crust) is representing the stretched and hot back-arc lithosphere of the Aegean domain. The background crust is placed everywhere, except when another continental or oceanic plate is defined. The overriding continental crust (representing Anatolia) is 30 km thick, 1400 km wide and 1800 km long. A weak zone (100 km width) has been inserted between the overriding and the subducting plates to reduce the friction in the subduction channel and facilitate subduction initiation (Sternai et al., 2014). In some models, two further weak zones (50 km width) are positioned in the areas where the tear in the slab in western Turkey is located and in front of the shore of eastern Turkey, to initiate the detachment during the subduction. They were placed according to the models, giving the best fit to the present-day location of the tear and break-off in the slab (Biryol et al., 2011). Relative convergence between the two plates is modelled by imposing a constant velocity (2 cm/yr) on the subducting plate ( $z = 0$ –2500 km) and by fixing the overriding continental plate at the rear ( $z = 1875$ –2500 km). The boundaries are periodic, normal to the x direction, no slip is imposed at the bottom boundary and free slip to the sides and top boundaries (Faccenda and Capitanio, 2013; Faccenda, 2014).

The thermal structure (Fig. 3) of the plates is calculated with the half-space cooling model, developed by (Gerya, 2009), down to 90 km, below a constant thermal gradient of 0.5 K/km is assumed. The upper plate is set to be 70 Myrs old in the continental portion (overriding) and 5 Myrs for the background lithosphere, which ensures its deformation and trench retreat, while the subducting and oceanic plate is 150 Myrs old. The oceanic crust, as well as the mantle and background crust have a visco-plastic rheology, based on deformation invariants (Ranalli, 1995; Faccenda, 2014). It has been modelled with wet Quartzite and dry Olivine flow laws, respectively (Table 1). The lower and upper cut-off values of the effective viscosities are  $10^{18}$  and  $10^{24}$  Pa s, respectively. To further decrease the strength of the upper plate material, its upper cut-off value has been set to  $10^{22}$  Pa s (Table 1). Density is computed as a function of the local P–T diagram generated with PERPLE\_X (Connolly, 2005) for a pyrolytic mantle composition. The low friction coefficient of the overriding continental plate (0.01) is needed to ensure yielding of the upper plate due to the used low numerical resolution that does not allow to localize deformation and behaves as a rigid block.

## 2.2. Mantle fabric modelling

The lattice preferred orientation (LPO) of mantle aggregates are modelled by using a modified version of D-REX (Kaminski et al., 2004). A detailed explanation for the LPO modelling can be found in Faccenda and Capitanio (2013). The Eulerian velocity gradient field from the large-scale mantle flow model is used to compute the fabric development of each crystal aggregate with an initial spacing of  $(x, y, z) = 50 \times 3050$  km at each time step. Since this study focuses on seismic SKS phase splitting as an observational constraint, we only model the anisotropy in the upper mantle (from the Moho to the 410 km discontinuity) to which the long period S-waves are sensitive. Thus, below 410 km no fabric is calculated, but the aggregates continue to be advected with their fabric reset. When emerging in the upper mantle (above 410 km) again a new fabric is computed. Each upper mantle aggregate consists of 1000 randomly oriented crystals (70% olivine, 30% pyroxene). We have used the standard D-Rex parameters to calculate the fabrics. Following Boneh et al. (2015) we set the grain-boundary-mobility (MOB, dimensionless) of olivine to 10, which yields weaker LPOs and associated seismic anisotropy more consistent with observations. Anisotropy of deformed upper mantle aggregates is dominated by the transverse isotropy (TI) component (Becker, 2006), where the olivine fast axis is parallel to the symmetry axis and the other two crystallographic axes are perpendicular to it. As such, the elastic properties of anisotropic aggregates are shown by plotting the symmetry axis of the TI component which is extracted automatically from the full elastic tensor by D-Rex.

## 2.3. Synthetic SKS splitting

Synthetic SKS splitting parameters are computed with FSTRACK (Becker, 2006) at the final timestep, using the full elastic tensors of the upper mantle crystal aggregates, vertically stacked below a given station (grid with 50 km spacing, down to 400 km in the central area of the model). We compute the harmonic response of the vertical stack of layers to an incident plane wave with 5° to the vertical, over a range of frequencies (0–25 Hz), to obtain a pulse seismogram via the inverse Fourier transform, using the method of Kennett (2009) with anisotropic extensions (Chapman and Shearer, 1989, and references therein). Band-pass filters from 0.1 to 0.3 Hz are then applied to construct synthetic seismograms in the SKS band (3.3 to 10 s). Successively, the splitting is determined with the cross-correlation method of Menke and Levin (2003). The SKS splitting parameters of each seismic station are obtained by averaging all the fast azimuths and delay times mea-

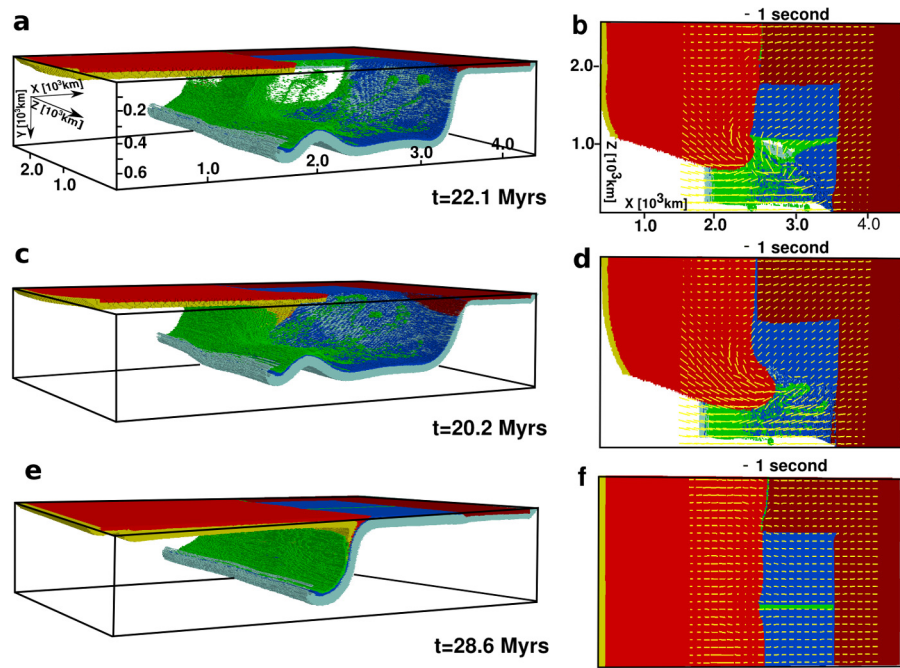


**Fig. 4.** 3-D view of three different models and resulting SKS splitting parameters (yellow lines). a, b model with weak zones in the subducting oceanic plate (T63, best fit model). c, d model without weak zones (T80). e, f model with a strong uniform upper continental plate (T79).

sured by rotating the vertical stack of elastic tensors by  $2^\circ$  intervals around the  $y$ -axis.

### 3. Results

#### 3.1. Different model geometries and kinematics

Although different parameters and material properties have been tested, a few selected and important models will be presented in this section (Fig. 4). In our best fitting model (T63, see, Supplementary Materials and Fig. 4a, b), the trench retreats by about 5 cm/yr in a timespan of 22.1 Myrs, while the subduction rate is about 2.3 cm/yr. The retreat starts at 3.3 Myrs with a rate of about 4 cm/yr and a slab dipping angle of about  $30\text{--}45^\circ$ . Starting at about 10 Myrs to 14.6 Myrs the retreat becomes very strong (15 cm/yr), but at the same time the slab becomes more gentle ( $30^\circ$ ). A tear as well as a break-off in the slab were achieved by imposing weak zones. The tearing starts around 14.6 Myrs. The slab steepens again rapidly afterwards to about  $60^\circ$ , implying the roll-back of the slab becomes faster, while the retreating velocity of the trench slows down ( $\approx 2.6$  cm/yr) until the last timestep. When arriving at the lower boundary of the model, the slab becomes horizontal and buckles. The overriding plate is extruding into the background lithosphere area with a counterclockwise motion after 12 Myrs. In the non-retreating subduction areas the dipping angle of the slab is about  $45^\circ$ . The collision of the subducting and overriding continental plates occurs around 14 Myrs, while the break-off happens at about 4 Myrs.

More than 80 models have been tested in this study. Very fast trench retreat rates (e.g. T14  $\approx 8$  cm/yr, T54  $\approx 6$  cm/yr) and late tearing (e.g. T54 at about 19 Myrs, after the subducting slab reaches the right subducting continental plate) in earlier models were prevented by e.g. increasing the age of the subducting oceanic plate to 150 Myrs and decreasing the activation volume to 1 J/bar, while horizontal subduction of the slab was avoided by increasing the friction coefficients as well as brittle strain weakening. A lower rigidity and thus higher deformation of the upper continental plate was obtained by decreasing the viscosities upper cut-off value by two orders of magnitudes. The  $x$ -normal periodic

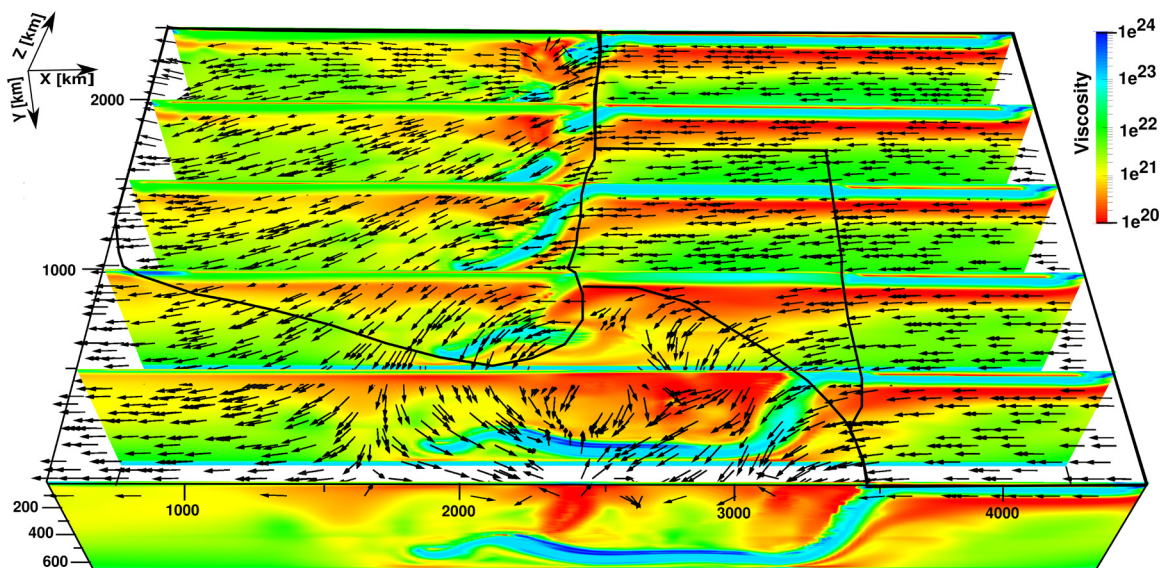
boundary conditions were found to be critical in order to have a sustained slab roll-back. Initially, the  $z$ -domain was set to 2000 km, but mantle flow and strain could not evolve independently in the roll-back area without being influenced by surrounding regions. To achieve this, 500 km were added to the width of the back-arc domain (oceanic subducting and continental subducting plate respectively).

Fig. 4c shows the geodynamic result after 20.2 Myrs of a model (T80) without weak zones. The retreat of the trench is fast ( $\approx 7$  cm/yr) and no detachment in the slab can be observed. The strong mantle flow through the tear is missing and the front part of the overriding plate appears to retreat very fast towards the right. The third model (T79) (Fig. 4e), with a wide overriding plate (strong continental crust) produces a steep slab without retreat, even after 28 Myrs years. The break-off in the top part of the model is achieved beneath a region where the weak zone is placed initially, although no tear propagation at the corner of the overriding continental plate and slab is observed.

#### 3.2. Mantle flow and viscosity/temperature field

The overall trend of the direction of mantle flow in the upper mantle, which is estimated at the end of the model evolution (model T63, Figs. 5, 6 and S1) underneath the subducting plate is parallel to the plate movement direction and becomes vertical when entrained at depth by the slab. As a result of the strongly retreating trench and the geometry of the plates, the overriding continental plate is laterally extruded towards the trench and the upper mantle flow below this plate is oriented counterclockwise at about  $25^\circ$  with respect to the convergence direction. Subduction induces poloidal convective cells below and above the slab, with upwelling at the slab tip, horizontal corner flow in the transition zone and return flow underneath the slab. Such toroidal and poloidal flow components are locally perturbed in proximity of the break-off and tear areas where the sub-slab mantle migrates fast toward the mantle wedge.

The viscosity (Fig. 5) is much lower in the mantle surrounding the sliding portions of subducting and overriding plates, owing to the employed non-Newtonian, strain rate dependent, rheology.



**Fig. 5.** Viscosity field on six vertical slices along the x-plane with 500 km spacing at 22.1 Myrs of model T63. Arrows are scalars of the flow direction on a horizontal slice in 100 km depth. Black lines represent sketch of plate boundaries and trench.

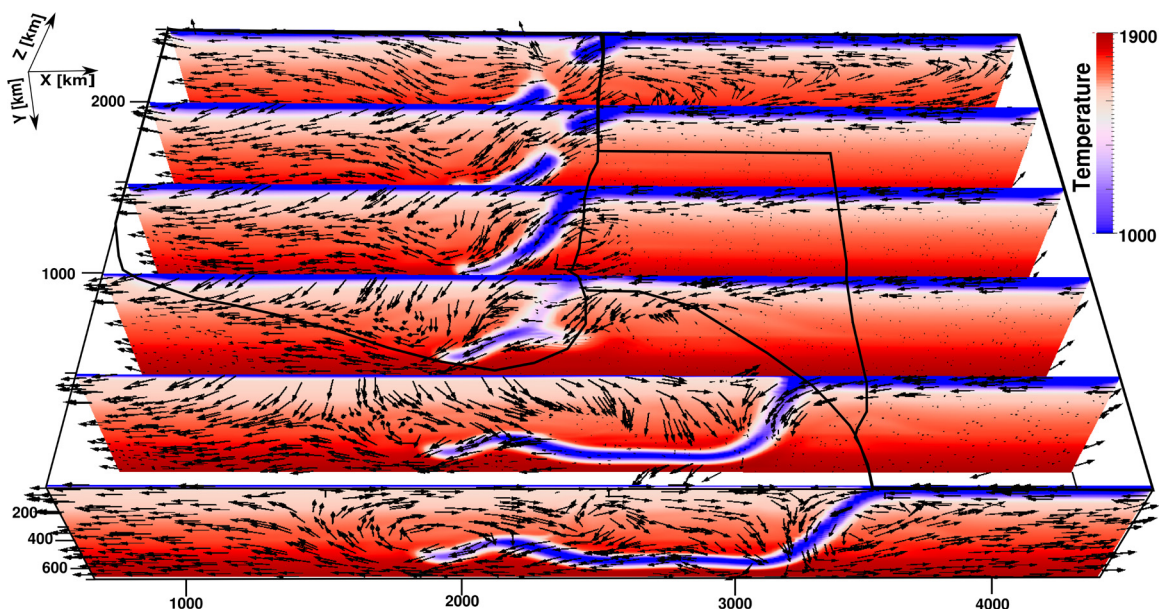


**Fig. 6.** Temperature field in Kelvin and flow direction (arrows) on six vertical slices along the x-plane with 500 km spacing at 22.1 Myrs of model T63. Black lines represent sketch of plate boundaries and trench.

Very low viscosity zones can be seen in the break-off and tearing area where the hot and actively deforming upper mantle penetrates in the mantle wedge through the slab window. The temperature field (Fig. 6) is more layer and depth dependent, owing to the adiabatic heating/cooling that suppresses thermal instabilities. Depth independent changes of temperature can be seen in proximity of the cold slab which is warming up very slowly. In the break-off and tear areas, hot material flows through the cold walls of the slab and heats the overlaying mantle lithosphere. The mantle flow of T80 (Fig. 4c) is similar to model T63 (reference model), except that there is no inflow of subslab mantle into the mantle wedge. As a result of this, the poloidal component of mantle flow increases at the expenses of the toroidal component. The subduction-induced mantle flow of model T79 (Fig. 4e) above and below the slab is predominantly poloidal as the slab kinematics is constant along the trench. Differential retreat/advance of the slab is needed to generate horizontal (toroidal) mantle flow.

### 3.3. Synthetic calculation of SKS anisotropy parameters

The strongest LPOs and related highest transverse isotropy in the upper mantle (10%, up to ten times higher than its neighbouring regions, Fig. 7) can be seen in the area surrounding the retreating slab from the top, down to a depth of 410 km, while the poorly deforming slab is isotropic. Underneath the subducting oceanic and continental plate anisotropy changes from maximum 10% in adjacent mantle levels to only 1% in deeper layers and the general trend is trench-perpendicular. Anisotropy is higher in the break-off and tear zones (6–8%). The symmetry axes are sub-parallel to the average orientation of the olivine fast axis (Faccenda and Capitanio, 2013) and to the mantle flow and strain directions.

SKS splitting parameters in our best model (T63) are mostly trench-perpendicular and show a circular pattern below the extruding overriding continental plate (Figs. 4b and 8). In the back-arc area very high TDs (up to 4 s) and trench-perpendicular FPDs

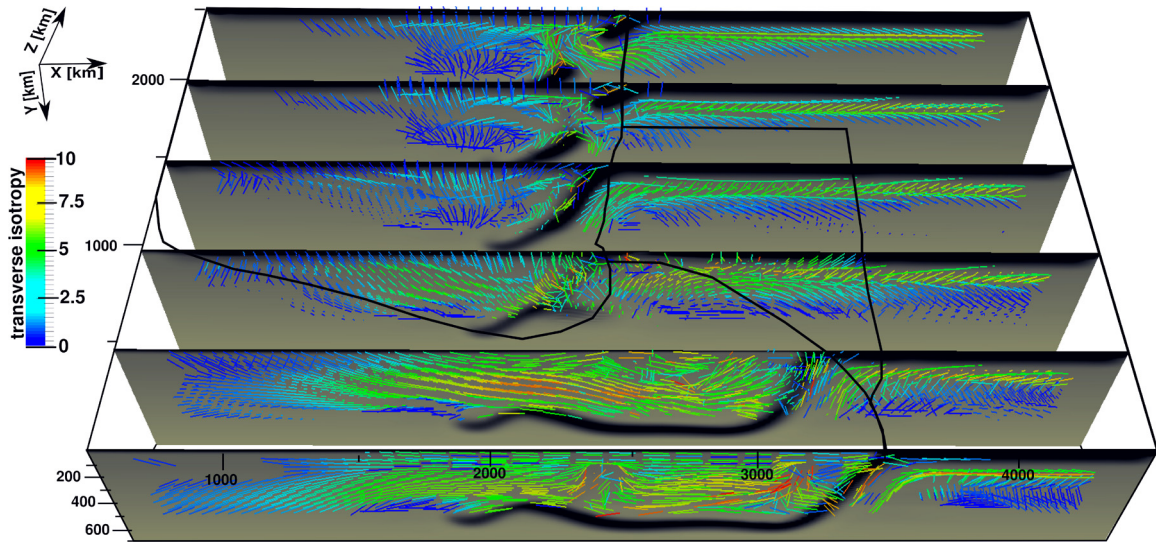


**Fig. 7.** 50 km thick slices mapping temperatures from low to high values (black to grey, respectively) and transverse isotropy (the bars indicating the direction of the symmetry axis), with the schematic sketch of the plate boundaries (black lines) at 22.1 Myrs of model T63. The colour and length of the bars is proportional to the amount of transverse isotropy.

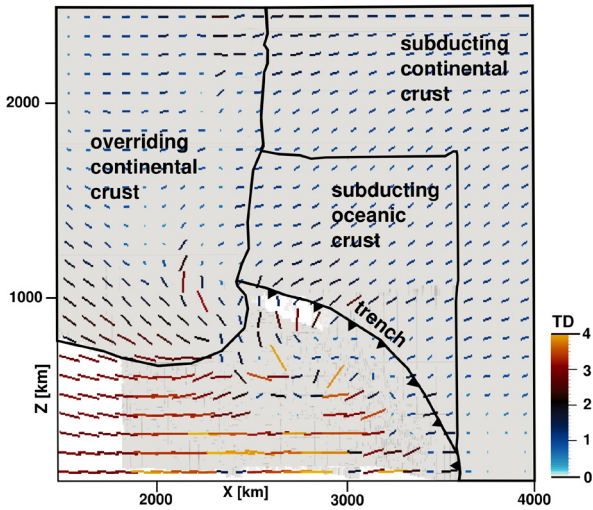


**Fig. 8.** SKS splitting parameters in a selected central area in the model with a 50 km spacing station grid of model T63. Colourbar shows the delay time in seconds.

exist, while splitting parameters closer to the trench are smaller ( $TD < 1$  s) with inconsistent FPDs. The sub-horizontal mantle flow through the tear produces very strong ( $TD = 2\text{--}3$  s) FPDs perpendicular close to the trench, but oblique to the overall trend in the back-arc area. Near the edges of the tear, the FPDs are affected by the fast mantle flow and display a circular pattern and higher time delays (2–3.5 s) than the surrounding areas (0.5–2 s). Similarly, the strong mantle flow in relation to the break-off in the top part of the model controls SKS splitting parameters with FPDs oriented strictly parallel to the flow and higher time delays ( $\sim 2$  s) than surrounding regions (1 s). On the other hand, the break-off does not have such a strong impact, since the main direction of flow and strain is similar to the converging direction.

SKS splitting parameters of model T80 (Fig. 4d) are quite similar to T63, only the splitting parameters affected by the tear and the strong movement of the front part of the continental overriding plate differ. This can be seen in even stronger and more organised counterclockwise rotating splitting parameters. In model T79 the time delays are very small (about 1 s) and splitting parameters align mainly perpendicular to the trenches, exceptions are only close to the weak zones (Fig. 4f).

## 4. Discussion

### 4.1. Model set-up, evolution of plate movement and mantle flow

Our numerically computed geodynamic model convincingly simulates the evolution and current geological situation of the eastern Mediterranean in many aspects. We favour our interpretation of the best fitting model, T63 (Fig. 4a, b), which includes a slab tear, a slab break-off and a fast retreating trench, since the proofs of these features have been evident in various seismic imaging studies (e.g. seismic tomography, receiver functions, shear wave splitting measurements, surface waves analysis). The model dimensions differ from the actual present-day geometry in many areas. For instance, the Aegean Sea is just about 500 km wide in E–W direction, but for resolution and modelling reasons we had to make it 1000 km wide (see 3.1). This allowed the halfcircle of retreat to establish its independent mantle flow and strain region, less influenced by boundary conditions and nearby regions. On the other hand, the width of Anatolia represented by the overriding continental plate is 2000 km as being similar to its present-day dimensions. Here we should notice that we primarily focus on the subduction systems and the outcome of mantle flow and anisotropy patterns and some adjustments had to be done to fit for example the resolution of the model and convergence rates. A change in geometries of the African and Arabian plates as well as the N–S width of the oceanic plate would not have a strong impact on mantle flow directions and splitting parameters since there has not been any drastic change of plate movement in the past 20 Myrs.

Recent strong extension in the Aegean (last 10–15 Myrs, Jolivet et al., 2013) and a tear in the slab between the Hellenic and the Cyprus trench (15 Myrs ago, Dilek and Altunkaynak, 2009; Jolivet et al., 2015), amplifying roll-back, can be dated likewise in our model about 12 Myrs and 8 Myrs before the last timestep (blt), respectively. The fast extension 12 Myrs blt in our model triggers the tearing (8 Myrs blt), afterwards the tension between overriding plate and oceanic plate is released, as a consequence the retreat slows down and the slab angle steepens. As postulated by Taymaz et al. (1990) the slab is dipping northward, but is more fragmented, than in our study. The dip angle of the retreating slab ( $60^\circ$ ) is steeper than the one observed in tomography models Biryol et al. (2011). The slab becomes even steeper following the initiation of the tearing. Whereas the eastern continuation

of the slab is dipping with an angle of  $45^\circ$  that is similarly resolved for the Cyprus slab of Biryol et al. (2011). Our model calculations date the collision of the continents in eastern Anatolia very late (8 Myrs blt). Thus comparing them with plate evolution models (e.g. Jolivet and Faccenna, 2000, about 30–35 Myrs ago) is difficult, due to the simplicity of starting models, that are supposed to involve the complicated history of long lasting subduction processes in the region. The break-off in the slab happens in our model at about 18 Myrs blt, which is earlier than in the literature (Keskin, 2003, 11–13 Myrs ago). These discrepancies arise from different subduction speeds and mechanism from west to east and combining them into a single model is difficult. However, we would like to notice here that our modelling study can provide important constraints on possible effects of these geodynamic events on mantle flow and strain history.

Our strong northward directed mantle flow velocity field through the break-off in eastern Turkey, the movement of the plates and counterclockwise rotating velocity vectors towards south match the movement of the upper plates of a laboratory tests carried out by Faccenna et al. (2006). Variations of our flow directions within the uppermost mantle ( $\approx 100$  km) (Figs. 5 and S1) and plate movement from GPS measurements (Reilinger et al., 2006; Le Pichon and Kreemer, 2010) agree in many regions, especially the Aegean, western Anatolia and the Arabian plate. In central and eastern Anatolia GPS vectors appear to show roughly  $30^\circ$  of eastward deviation with respect to our mantle flow vectors at a depth of 100 km. This general consistency might be an indicator of a possible coupling between the crust and the uppermost mantle as earlier proposed by Göğüş and Pysklywec (2008), not just for eastern Anatolia but a larger region including central and western Anatolia and the Aegean. Starting at a depth of 300 km, mantle flow vectors are mostly oriented parallel to the subduction direction in Anatolia and affected strongly by the tearing and break-off, as well as toroidal corner flow with trench-parallel mantle flow underneath and behind the slab.

#### 4.2. Selection of optimum model

Numerous models were tested searching for the best fitting rheological properties and plate tectonic features in the study region. Finally we decided on T63 as the optimum match following a weighting process between a realistic reconstruction and numerical modelling limitations. In this section we will discuss why we eliminated some other typical model setting for further interpretation.

A model without imposed weak zones (T80, Fig. 4c), to start detachment, but otherwise same rheological properties as the reference model T63, shows no sign of tearing or break-off. The impact on mantle flow and anisotropy, of missing slab openings, is only noticeable underneath these detachment areas. In T63 the tearing slows down the otherwise fast extrusion towards the trench, which seems to be too extreme in T80. A tear in the slab underneath western Anatolia (e.g. Jolivet et al., 2015; Govers and Fichtner, 2016) and a break-off in the slab in eastern Anatolia (e.g. Göğüş and Pysklywec, 2008; Faccenna et al., 2006) appear to be common features of the literature. Placing weak-zones might not represent a realistic geological scenario, due to unrealistic high friction coefficient and low viscosity parameters for crustal depths, but it seems to be an important modelling gadget, to reproduce detachment in the slab.

Due to the absence of roll-back and tear initiation in the retreating area, model T79 (Fig. 4e) does not fit the recent evolution of the Aegean. For a good reconstruction of the mantle flow and strain in this region, the fast retreat is necessary, for higher TDs and toroidal flows. Inserting a thicker continental crust than in T63 might represent the crustal thickness of the Aegean (Tirel et al.,

2004) better, but the numerical modelling implication is difficult. Therefore we decided to focus on the evolution of the mantle flow and anisotropy, rather than implementing the exact crustal dimensions.

#### 4.3. Seismic anisotropy

The general pattern of the synthetic 3-D anisotropy calculations (Fig. 8), with a complex subduction model geometry and fitting parameters for the crust and upper mantle, imitating the eastern Mediterranean and Anatolian region, resemble to a first order, existing measured data in the area (Figs. 2 and 9). N–S (back-arc region/Aegean) to NE–SW (overriding/Anatolian plate) oriented FPDs are dominant over a broad area as observed in early SKS studies that have sampled eastern Turkey (e.g. Sandvol et al., 2003), north-central Turkey (Biryol et al., 2010), western Turkey (Paul et al., 2014), the Aegean Sea (Evangelidis et al., 2011; Confal et al., 2016) and along the Cyprus trench (Yolsal-Çevikbilen, 2014). Since symmetry (free-slip) conditions are applied to the front boundary ( $z = 0$ ) of the model, the trench is confined only in a half-arc, rather than the curved Hellenic trench. Thus, synthetically computed FPDs in the back-arc region are about  $20$ – $30^\circ$  more inclined towards north than those observed in most of the SKS studies.

The LPO simulations have several limitations, as for example they assume A-type olivine throughout the upper mantle domain, although melt, aqueous fluids and high stresses atop the subducting slab might favour the formation of different olivine fabrics (e.g. Jung et al., 2006) and/or the appearance of strongly anisotropic hydrous phases. Furthermore, the models do not take into account changes in creep mechanism and single crystal elastic properties as a function of the local pressure and temperature conditions which affect the seismic anisotropy signal. The D-Rex parameters have been calibrated with low strain deformation experiments (Kaminski et al., 2004, and references therein), but a comparison with high strain fabrics (e.g. Hansen et al., 2012) is still lacking. As a matter of fact, and similarly to what has been previously found (Becker, 2006; Faccenna and Capitanio, 2013), a good fit between the synthetic data and the observations is achieved when the mantle flow is sub-horizontal. This is because the average orientation of the olivine fast axis is also horizontal, producing the largest anisotropy contribution for the vertically travelling SKS wave. Altogether, these limitations might be the principal reason for the overestimation of the TDs in the synthetic Aegean area and for the poor fit of the SKS data around the trench where the vertical component of flow is large.

We should also notice here that SKS-derived FPDs represent path-integrated average anisotropy parameters over depth and time, and therefore might differ from mantle flow directions. The anisotropy pattern in the Aegean is complicated and appears to be affected by a layered structure with depth-varying anisotropic features. For a better comparison, a well-resolved variation of vertically stratified azimuthal anisotropy that could be inferred from the inversion of surface waves (e.g. Rayleigh waves) is necessary. Such information has been available, until now, for a limited part of the study area in Endrun et al. (2011) and must be expanded further to the north and east by covering the entire Aegean and Turkey.

##### 4.3.1. Slab roll-back – Aegean back-arc region

Splitting parameters with very high time delays (up to 4 s for synthetic vs. 2 s for measured data) and trench-perpendicular FPDs can be observed in the area of the retreating slab, due to the existence of several or thick layers with identical FPDs increasing the strength of anisotropy and thus time delays. The 2 s time delay discrepancies between synthetic and observed time delays could be caused by several reasons: i) our strain-induced mantle fabrics

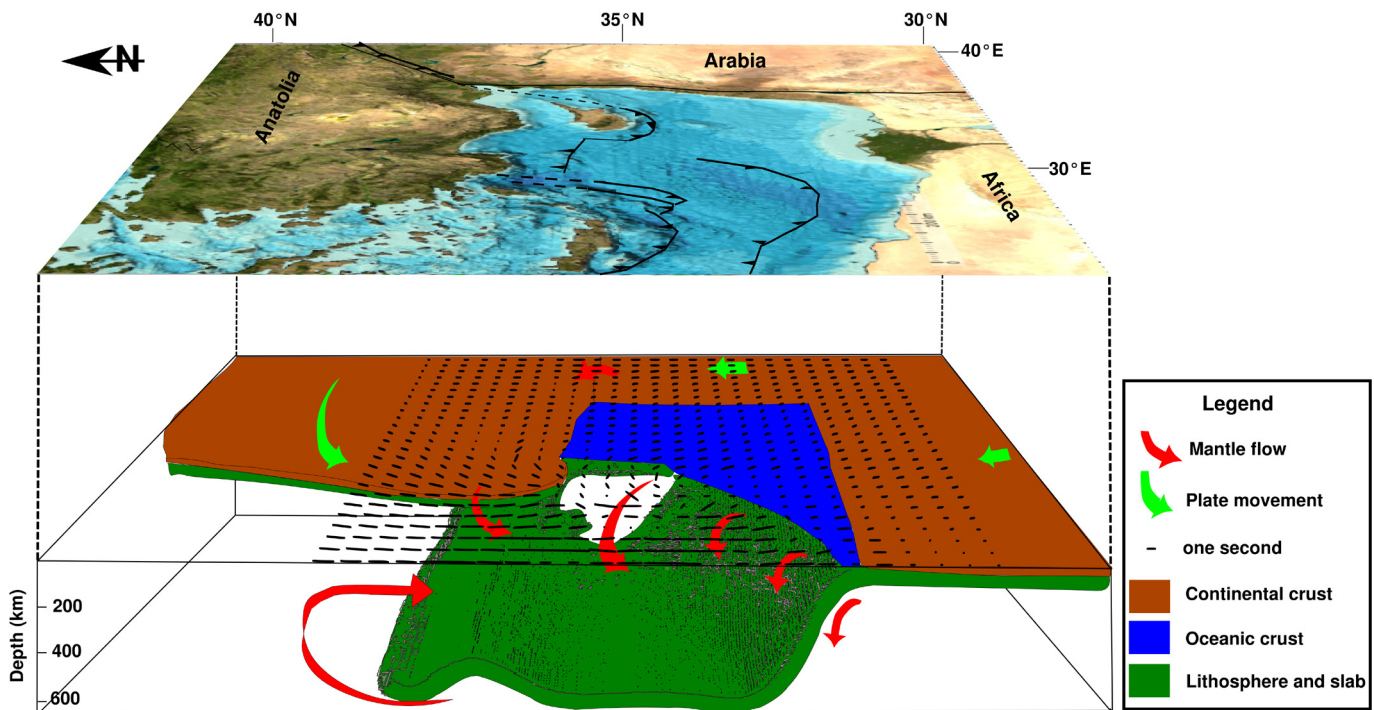


**Fig. 9.** Geodynamic interpretation and modelled SKS splitting parameters (black lines, scale in 1 s) at the last timestep with the present-day map view of the eastern Mediterranean on top (GeoMapApp, <http://www.geomapp.org>). Important tectonic features are represented in the map view with a rough sketch. Red arrows represent the mantle flow interpreted from this study and green arrows show the plate movement.

are too strong, indicating the active dislocation creep at shallow depths (e.g. Karato et al., 2008), ii) upper mantle minerals become more isotropic with depth, iii) a more complex mantle flow exists in the Aegean area as it produces destructive interference among the different mantle layers. Other modelling studies (e.g. Faccenna et al., 2013) estimated very small TDs (average 0.5 s) but similar orientations, likely because of a minor amount of time-integrated deformation imposed to develop the fabrics. Most recent studies considering a reliable amount of events exhibit at least TDs of 1 s and higher (e.g. Paul et al., 2014; Confal et al., 2016).

Likewise anisotropic directions resolved after the anisotropic inversion of Rayleigh waves in Endrun et al. (2011), we identified significant N–S directed FPDs in the mantle lithosphere of the North-Aegean Sea. Anisotropy patterns in the Aegean (strong TDs and trench-perpendicular FPDs) seem to be mainly controlled by corner flow, return flow and high strain rates due to extensional conditions. The return flow in the sub-slab region and corner flow above the slab are very well resolved in our mantle flow model (Figs. 6, 9 and S1). The corner flow might be too strong and pushing the slab in a steeply dipping direction. The N–S directed FPDs in the back-arc region, compared to NE–SW FPDs in measured data, exist because free slip is applied to the sides of the model.

On the other hand, SKS splitting parameters in the fore-arc are smaller ( $TD < 1$  s) and chaotic with some trench-parallel FPDs. Based on a globally compiled SKS splitting measurement data, Long and Silver (2009) reported that many subduction zone environments indicate a similar pattern. Yet, Faccenna and Capitanio (2013) more recently reported that this might only occur at narrow and retreating slabs. Since our system is retreating relatively fast and narrow this hypothesis would be reasonable. But only a few stations exhibit trench-parallel FPDs in the measured data (Evangelidis et al., 2011). However, these stations might be misleading according to Confal et al. (2016) due to the limited number of individual SKS observations (e.g. 3–4). Relatively small time delays close to the trench and seaward ( $TD < 1$  s) could be due to the effect of differently oriented anisotropy in the mantle layers.

#### 4.3.2. Slab tear – western Anatolia

As noticed by Paul et al. (2014), there is a change in south-western Anatolia to NW–SE oriented FPDs, due to the flow of asthenospheric material into the mantle wedge. This phenomena can be observed in the circular pattern at the edges of the tear and high TDs in our model as well. The location of the tear in the slab, regarding to Biryol et al. (2011), is further underneath the continental plate than in the geodynamic model of this study. But according to Govers and Fichtner (2016), the slab started tearing underneath Anatolia and then travelled southward, similarly to our modelled slab tearing, which started underneath the lower margin of the upper continental crust (representing south-western Anatolia) and propagated toward the right boundary. Nevertheless, calculated and measured splitting parameters show FPDs rotating from trench-normal (central continental plate) to a counterclockwise pattern, at the edge of the tear, leading towards the back-arc area. The high heat flow associated with the vertical tear in south-western Turkey could explain Late Miocene and Pliocene volcanism (Dilek and Altunkaynak, 2009). Since then, extensional tectonics became more important for magmatic activities than the slab tearing.

#### 4.3.3. Slab break-off – eastern Anatolia

In eastern Turkey, the synthetic model of the mantle flow through the break-off in the slab shows a significant contribution to the geodynamics of the region and higher time delays point to strong mantle flow. Warmer material from beneath the slab in the asthenosphere is transported to upper layers in the lithosphere (Fig. 6). The coverage of splitting data in eastern Turkey is sparse, but Sandvol et al. (2003) and Paul et al. (2014) showed that FPDs are mostly oblique (NE–SW) towards the Bitlis–Zagros Suture zone and normal in the East due to the curvature of the suture zone, while our model data is N–S directed and strictly perpendicular to the suture zone. Such difference could be associated to the boundary conditions of our model (free slip normal to  $z$  and periodic normal to  $x$ ) or to the larger-scale mantle flow dynamics resulting

from the effect of existence of a broader Arabian–Eurasian collision zone, which is not modelled in this study. The consistency of observed and synthetic SKS splitting data and the mismatch between anisotropic orientations and surface features along the suture zone support the idea that the anisotropy in the region is related to ongoing deformation in the asthenosphere, rather than representing fossil anisotropy in mantle lithosphere (Babuska and Cara, 1991). The change of N–S directed mantle flow south of the suture zone to NW–SE (similar to Capitanio, 2016) and low viscosities could explain the westward escape of the Anatolian microplate (Figs. 5, 6 and S1). This does not mean that there could not be any pull due to the roll-back in the Aegean, but rather that they might be connected. Further anisotropic modelling, including vertical stratification of layers, is required in this region to better constrain strain-induced LPO in the past or at present. Nevertheless, the flow through the break-off could explain volcanism, domal uplift, heating and extension as described in several studies (e.g. Keskin, 2003; Göğüş and Pysklywec, 2008; Fichtner et al., 2013; Govers and Fichtner, 2016).

Our results show a good accordance with alternative anisotropic modelling study of Faccenna et al. (2013) covering a larger region, but our modelling study adds more details especially in western and central Anatolia.

## 5. Conclusion

In this study we reproduce the present-day anisotropy patterns in the Aegean Sea, around the Cyprus trench as well as in Anatolia. To achieve this, upper mantle anisotropy and synthetic SKS splitting parameters were calculated with three different algorithms (I3MG, D-REX and FSTRACK) by modelling the 3-D geodynamics of the eastern Mediterranean and Anatolian subduction systems, the strain-induced LPO in the upper mantle and seismic wave propagation. We show that this combination of calculations can achieve SKS splitting parameters similar to observed data. Below the extruding Anatolian plate, the general FPDs are NE–SW directed, and circular around the tear in the slab, while strong splitting can be noticed in the Aegean region.

Differences between synthetic SKS splitting parameters and real data could be ascribed to the imposed model geometry and boundary conditions, potential effects related to larger-scale flow patterns and/or nearby subduction systems and different rheological parameters which control plastic deformation of upper mantle minerals. As an example, the presence of a highly fragmented slab would substantially affect on a local scale the geology and seismic anisotropy parameters.

Nevertheless, our study demonstrates that this type of combined simulations can reproduce to a first order the time-dependent 3-D patterns of mantle convection and resulting seismic anisotropy is mainly consistent with measured observations.

## 6. Data and resources

Geodynamic simulations were performed on Galileo Computing Cluster, CINECA, Italy. The I3MG (Gerya, 2009) code was used for the geodynamic modelling, D-Rex (Kaminski et al., 2004) for the fabric modelling and FSTRACK (Becker, 2006) to calculate SKS splitting parameters. Paraview was used for graphic visualization (<https://www.paraview.org/>). Data from prior SKS splitting measurements were taken from Wüstefeld and Bokelmann (2007). The figures are generated using the Generic Mapping Tools software (GMT, <http://gmt.soest.hawaii.edu/projects/gmt>) and Inkscape.

## Acknowledgements

This study is part of an ongoing Ph.D. thesis, by Judith M. Confal, which is funded by the National Scientific and Technolog-

ical Research Council of Turkey (TÜBİTAK), project no: ÇAYDAG-115Y248. We are thankful to the University of Padova, Italy, for supporting the research, with the permission for the use of the Galileo Computing Cluster, CINECA. We thank the Turkish Academy of Sciences (TÜBA) in the framework for Young Scientist Award Program (TÜBA-GEBİP) and the Alexander von Humboldt Foundation Research Fellowship Award for financial support and for further providing computing facilities and other relevant resources through Humboldt-Stiftung Follow-Up Programme. This paper has benefited from the review of A. Menant and an anonymous reviewer.

## Appendix A. Supplementary material

Supplementary material related to this article can be found online at <https://doi.org/10.1016/j.epsl.2018.06.005>.

## References

- Babuska, V., Cara, M., 1991. *Seismic Anisotropy in the Earth*, vol. 10. Springer Science & Business Media.
- Becker, T.W., 2006. On the effect of temperature and strain-rate dependent viscosity on global mantle flow, net rotation, and plate-driving forces. *Geophys. J. Int.* 167, 943–957.
- Biryol, C.B., Beck, S.L., Zandt, G., Özacar, A.A., 2011. Segmented African lithosphere beneath the Anatolian region inferred from teleseismic P-wave tomography. *Geophys. J. Int.* 184, 1037–1057.
- Biryol, C.B., Zandt, G., Beck, S.L., Özacar, A.A., Adiyaman, H.E., Gans, C.R., 2010. Shear wave splitting along a nascent plate boundary: the North Anatolian Fault Zone. *Geophys. J. Int.* 181, 1201–1213.
- Boneh, Y., Morales, L.F., Kaminski, E., Skemer, P., 2015. Modeling olivine CPO evolution with complex deformation histories: implications for the interpretation of seismic anisotropy in the mantle. *Geochem. Geophys. Geosyst.* 16, 3436–3455.
- Capitanio, F.A., 2016. The role of the miocene-to-pliocene transition in the eastern Mediterranean extrusion tectonics: constraints from numerical modelling. *Earth Planet. Sci. Lett.* 448, 122–132.
- Chapman, C., Shearer, P., 1989. Ray tracing in azimuthally anisotropic media-II. Quasi-shear wave coupling. *Geophys. J. Int.* 96, 65–83.
- Confal, J.M., Eken, T., Tilmann, F., Yolsal-Çevikbilen, S., Çubuk-Sabuncu, Y., Saygin, E., Taymaz, T., 2016. Investigation of mantle kinematics beneath the Hellenic-subduction zone with teleseismic direct shear waves. *Phys. Earth Planet. Inter.* 261, 141–151.
- Connolly, J.A., 2005. Computation of phase equilibria by linear programming: a tool for geodynamic modeling and its application to subduction zone decarbonation. *Earth Planet. Sci. Lett.* 236, 524–541.
- Çubuk-Sabuncu, Y., Taymaz, T., Fichtner, A., 2017. 3-D crustal velocity structure of western Turkey: constraints from full-waveform tomography. *Phys. Earth Planet. Inter.* 270, 90–112.
- Dilek, Y., Altunkaynak, Ş., 2009. Geochemical and temporal evolution of Cenozoic magmatism in western Turkey: mantle response to collision, slab break-off, and lithospheric tearing in an orogenic belt. *Geol. Soc. (Lond.) Spec. Publ.* 311, 213–233.
- Endrun, B., Lebedev, S., Meier, T., Tirel, C., Friederich, W., 2011. Complex layered deformation within the Aegean crust and mantle revealed by seismic anisotropy. *Nat. Geosci.* 4, 203–207.
- Evangelidis, C., 2017. Seismic anisotropy in the Hellenic subduction zone: effects of slab segmentation and subsurface mantle flow. *Earth Planet. Sci. Lett.* 480, 97–106.
- Evangelidis, C., Liang, W.-T., Melis, N., Konstantinou, K., 2011. Shear wave anisotropy beneath the Aegean inferred from SKS splitting observations. *J. Geophys. Res., Solid Earth* (1978–2012) 116.
- Faccenna, M., 2014. Mid mantle seismic anisotropy around subduction zones. *Phys. Earth Planet. Inter.* 227, 1–19.
- Faccenna, M., Capitanio, F., 2013. Seismic anisotropy around subduction zones: insights from three-dimensional modeling of upper mantle deformation and SKS splitting calculations. *Geochem. Geophys. Geosyst.* 14, 243–262.
- Faccenna, C., Becker, T.W., Jolivet, L., Keskin, M., 2013. Mantle convection in the Middle East: reconciling Afar upwelling, Arabia indentation and Aegean trench rollback. *Earth Planet. Sci. Lett.* 375, 254–269.
- Faccenna, C., Bellier, O., Martinod, J., Piromallo, C., Regard, V., 2006. Slab detachment beneath eastern Anatolia: a possible cause for the formation of the North Anatolian fault. *Earth Planet. Sci. Lett.* 242, 85–97.
- Faccenna, C., Jolivet, L., Piromallo, C., Morelli, A., 2003. Subduction and the depth of convection in the Mediterranean mantle. *J. Geophys. Res., Solid Earth* 108.
- Fichtner, A., Saygin, E., Taymaz, T., Cupillard, P., Capdeville, Y., Trampert, J., 2013. The deep structure of the North Anatolian fault zone. *Earth Planet. Sci. Lett.* 373, 109–117.

- Gerya, T., 2009. Introduction to Numerical Geodynamic Modelling. Cambridge University Press.
- Göğüş, O.H., Pysklywec, R.N., 2008. Mantle lithosphere delamination driving plateau uplift and synconvergent extension in eastern Anatolia. *Geology* 36, 723–726.
- Govers, R., Fichtner, A., 2016. Signature of slab fragmentation beneath Anatolia from full-waveform tomography. *Earth Planet. Sci. Lett.* 450, 10–19.
- Hansen, L., Zimmerman, M., Kohlstedt, D., 2012. Laboratory measurements of the viscous anisotropy of olivine aggregates. *Nature* 492, 415.
- Jolivet, L., Faccenna, C., 2000. Mediterranean extension and the Africa–Eurasia collision. *Tectonics* 19, 1095–1106.
- Jolivet, L., Faccenna, C., Huet, B., Labrousse, L., Le Pourhiet, L., Lacombe, O., Lecomte, E., Burov, E., Denele, Y., Brun, J.-P., et al., 2013. Aegean tectonics: strain localisation, slab tearing and trench retreat. *Tectonophysics* 597, 1–33.
- Jolivet, L., Menant, A., Sternai, P., Rabillard, A., Arbaret, L., Augier, R., Laurent, V., Beaudoin, A., Grasemann, B., Huet, B., et al., 2015. The geological signature of a slab tear below the Aegean. *Tectonophysics* 659, 166–182.
- Jung, H., Katayama, I., Jiang, Z., Hiraga, T., Karato, S.-I., 2006. Effect of water and stress on the lattice-preferred orientation of olivine. *Tectonophysics* 421, 1–22.
- Kaminski, E., Ribe, N.M., Browaeys, J.T., 2004. D-Rex, a program for calculation of seismic anisotropy due to crystal lattice preferred orientation in the convective upper mantle. *Geophys. J. Int.* 158, 744–752.
- Karato, S.-i., Jung, H., Katayama, I., Skemer, P., 2008. Geodynamic significance of seismic anisotropy of the upper mantle: new insights from laboratory studies. *Annu. Rev. Earth Planet. Sci.* 36, 59–95.
- Kennett, B., 2009. *Seismic Wave Propagation in Stratified Media*, Cambridge University, ANU E Press.
- Keskin, M., 2003. Magma generation by slab steepening and breakoff beneath a subduction-accretion complex: an alternative model for collision-related volcanism in Eastern Anatolia, Turkey. *Geophys. Res. Lett.* 30.
- Kind, R., Eken, T., Tilmann, F., Sodoudi, F., Taymaz, T., Bulut, F., Yuan, X., Can, B., Schneider, F., 2015. Thickness of the lithosphere beneath Turkey and surroundings from S-receiver functions. *Solid Earth* 6, 971.
- Le Pichon, X., Kreemer, C., 2010. The Miocene-to-present kinematic evolution of the eastern Mediterranean and Middle East and its implications for dynamics. *Annu. Rev. Earth Planet. Sci.* 38, 323–351.
- Long, M.D., Silver, P.G., 2009. Mantle flow in subduction systems: the slab flow field and implications for mantle dynamics. *J. Geophys. Res., Solid Earth* (1978–2012) 114.
- Menant, A., Sternai, P., Jolivet, L., Guillou-Frottier, L., Gerya, T., 2016. 3D numerical modeling of mantle flow, crustal dynamics and magma genesis associated with slab roll-back and tearing: the eastern Mediterranean case. *Earth Planet. Sci. Lett.* 442, 93–107.
- Menke, W., Levin, V., 2003. The cross-convolution method for interpreting SKS splitting observations, with application to one and two-layer anisotropic Earth models. *Geophys. J. Int.* 154, 379–392.
- Mutlu, A.K., Karabulut, H., 2011. Anisotropic Pn tomography of Turkey and adjacent regions. *Geophys. J. Int.* 187, 1743–1758.
- Olive, J.-A., Pearce, F., Rondenay, S., Behn, M.D., 2014. Pronounced zonation of seismic anisotropy in the Western Hellenic subduction zone and its geodynamic significance. *Earth Planet. Sci. Lett.* 391, 100–109.
- Park, J., Levin, V., 2002. Seismic anisotropy: tracing plate dynamics in the mantle. *Science* 296, 485–489.
- Pasyanos, M.E., Walter, W.R., 2002. Crust and upper-mantle structure of North Africa, Europe and the Middle East from inversion of surface waves. *Geophys. J. Int.* 149, 463–481.
- Paul, A., Karabulut, H., Mutlu, A.K., Salaün, G., 2014. A comprehensive and densely sampled map of shear-wave azimuthal anisotropy in the Aegean–Anatolia region. *Earth Planet. Sci. Lett.* 389, 14–22.
- Ranalli, G., 1995. *Rheology of the Earth*. Springer Science & Business Media.
- Reilinger, R., McClusky, S., Vernant, P., Lawrence, S., Ergintav, S., Cakmak, R., Ozener, H., Kadirov, F., Guliev, I., Stepanyan, R., et al., 2006. GPS constraints on continental deformation in the Africa–Arabia–Eurasia continental collision zone and implications for the dynamics of plate interactions. *J. Geophys. Res., Solid Earth* 111, B05411.
- Sandvol, E., Turkelli, N., Zor, E., Gok, R., Bekler, T., Gurbuz, C., Seber, D., Barazangi, M., 2003. Shear wave splitting in a young continent–continent collision: an example from eastern Turkey. *Geophys. Res. Lett.* 30.
- Sternai, P., Jolivet, L., Menant, A., Gerya, T., 2014. Driving the upper plate surface deformation by slab rollback and mantle flow. *Earth Planet. Sci. Lett.* 405, 110–118.
- Taymaz, T., 1996. S–P-wave traveltimes residuals from earthquakes and lateral inhomogeneity in the upper mantle beneath the Aegean and the Hellenic Trench near Crete. *Geophys. J. Int.* 127, 545–558.
- Taymaz, T., Jackson, J., Westaway, R., 1990. Earthquake mechanisms in the Hellenic Trench near Crete. *Geophys. J. Int.* 102, 695–731.
- Tirel, C., Gueydan, F., Tiberi, C., Brun, J.-P., 2004. Aegean crustal thickness inferred from gravity inversion. *Geodynamical implications. Earth Planet. Sci. Lett.* 228, 267–280.
- Van Hinsbergen, D.J.J., Hafkenscheid, E., Spakman, W., Meulen Kamp, J., Wortel, R., 2005. Nappe stacking resulting from subduction of oceanic and continental lithosphere below Greece. *Geology* 33, 325–328.
- Vanacore, E., Taymaz, T., Saygin, E., 2013. Moho structure of the Anatolian Plate from receiver function analysis. *Geophys. J. Int.* 193, 329–337.
- Wortel, M., Spakman, W., 2000. Subduction and slab detachment in the Mediterranean–Carpathian region. *Science* 290, 1910–1917.
- Wüstefeld, A., Bokelmann, G., 2007. Null detection in shear-wave splitting measurements. *Bull. Seismol. Soc. Am.* 97, 1204–1211.
- Yolsal-Çevikbilen, S., 2014. Seismic anisotropy along the Cyprian arc and north-east Mediterranean Sea inferred from shear wave splitting analysis. *Phys. Earth Planet. Inter.* 233, 112–134.